Experimental Investigation of Mode-I Fracture Properties of Parallel Strand Bamboo Composite

Aiping Zhou,*[a,c] Zirui Huang,[b,c] Yurong Shen,[a,c] Dongsheng Huang,[a,c] and Jianuo Xu [d]

Parallel stand bamboo (PSB) is a high-quality wood-like bamboo composite. Failure due to cracking is a major concern in the design of PSB components for building structures. The mode-I fracture properties of PSB composite were studied. The wedge splitting method was employed as the test approach. Numerical analyses were conducted to determine the appropriate test specimen dimensions so that valid fracture toughness could be obtained. An R-curve was evaluated in accordance with the equivalent linear elastic fracture mechanics (LEFM) theory. It was found that the initial crack depth ratio should be less than 0.4 for the fracture toughness test. The fracture toughness of PSB is higher than that of commonly used woods, and their fracture behavior is similar, exhibiting quasi-brittle behavior. The R-curve of the PSB exhibits rising behavior until the critical crack length is reached. However, the post-peak R-curve exhibits a descending behavior, contrary to that of quasi-brittle materials, which present a plateau in post-peak crack extension.

Keywords: Fracture; Fracture toughness; R-curve; Energy release rate; Bamboo composite

*Contact information: a: School of Civil Engineering, Nanjing Forestry University 159#, Longpan Road, Nanjing, 210037, China; b: School of Civil Engineering, Southeast University, 02, Sipailou, Nanjing, 210018, P.R. China; c: National-Provincial Joint Engineering Research Center of Electromechanical Product Packaging with Biomaterials, Nanjing Forestry University 159#, Longpan Road, Nanjing, 210037, China; d: School of Architecture, Nanjing TECH University, 30#, Puzhu Road, Nanjing, 211800, China; *Corresponding author: zaping2007@163.com*

INTRODUCTION

Parallel strand bamboo (PSB) is a wood-like bamboo-based composite fabricated from bamboo strands. To manufacture PSB, bamboo culms are first cut into strips that are approximately 2 m in length, 15 mm in width, and 2 mm in thickness and then oven dried at 80 °C until the moisture content is less than 11%. The end product is made by flattening the strips into thin strands, impregnating them with phenolic resin, and gluing them in a parallel fashion under high pressure. Because the bamboo strands are laid in a parallel fashion in the longitudinal direction and are uniformly arranged in the transverse direction, the gradient distribution of fibers in raw bamboo is eliminated; hence PSB can be reasonably treated as a transversely isotropic composite in the macroscopic sense. PSB has excellent mechanical properties, and its products are well suited for use as construction material (Huang *et al*. 2013, 2015a,b).

Due to the dimensional diversity of strands or bamboo fibers, some gaps between the interfaces of the strands or fibers cannot be absolutely closed in the manufacturing process. Consequently, microvoids and fine cracks are randomly scattered in the PSB composite. Once a PSB component is loaded, these microvoids will coalesce and expand to form cracks. Because the strength of the fibers is much higher than that of the matrix, these cracks usually propagate along the parallel-to-grain direction and cause mode-I,

mode-II, or mixed mode fractures, depending on the loading responses of the components. Thus, the failure due to crack propagating is a major concern in the design of PSB components. Structural and fracture properties should be introduced to the failure criteria of PSB components in future designs. To this end, the present work is aimed at studying mode-I fracture properties of PSB composites. The wedge splitting method was employed to investigate the fracture toughness and failure mechanisms of PSB composites.

The application of conventional fracture mechanics, which deal with homogeneous, isotropic materials, and anisotropic composites, began with efforts to design load bearing structures in wood (Hearmon 1969). In particular, early aircraft structures contained wood, resulting in great interest in calculating stress concentration factors around holes (Williams 1989). By extending Lekhnitskii's method (Lekhnitskii 1963) to the fracture analysis for anisotropic media, Sith *et al*. (1965) developed a model to analyze the near-tip field of an edged or centered crack in an infinite sheet. Closed solutions for the near-tip stress and displacement fields as well as the stress intensity factors (SIFs) and the energy release rate for these cases were analytically obtained. According to Sith's theory (Sith *et al*. 1965), the stress intensity factors may be determined by contour integral around the crack tip. In most cases, however, the media containing a crack cannot be treated as an infinite body because the size of the crack is not small enough. The near-tip fields in these cases are strongly affected by dimensions and remote conditions and are difficult to determine due to mathematical complexity. Similar to Williams's (1957, 1952) works on isotropic materials, Sith's formulas for near-tip fields have only theoretical meanings. However, the relationship between the near-tip contour integral, J, and the stress intensity factor, K, proposed by Sith can be practically used to evaluate stress intensity factors for anisotropic media with various configurations.

Due to difficulties in determining the near-tip field of a crack, energy methods are widely accepted to evaluate the stress intensity factor in linear fracture mechanics. Based on the energy balance theory proposed by Griffith (1920), Iwrin (1956) defined a measure known as the energy release rate to quantify the energy balance for a unit area during crack extension. Rice (1968) investigated the energy flow around crack tips and provided a basis to evaluate the fracture toughness with an energy approach. Known as the J-integral method, this approach enjoyed great success in both anisotropic and isotropic materials. The J-integral approach provides a straightforward experimental method for evaluating J derived from its definition as a rate of change of potential energy with crack length. To estimate the energy release rate, some methods were developed to evaluate the fracture toughness without involving the near-tip field (Anderson 2005). The most common procedure among these methods may be the double cantilever beam (DCB) test. By changing the loading condition or the length ratio of the two cantilevers, the DCB specimen can be tested for mode-I, mode-II, and mixed-mode failures. For the mode-I test, the energy release rate of the DCB specimen can be inferred from beam theory. The advantages of the DCB test are obvious in that many intractable problems, such as the singularity of the crack tip, the anisotropy of materials, and the rigorous measurement of the crack length, are ignored. As far as PSB composites are concerned, the material stiffness is much lower compared to metallic materials, which results in large deformations in the DCB test and consequently leads to erroneous estimates of the energy release rate.

Compact specimen tests, recommended by the most major fracture test standards around the world, such as the American standard, ASTM E 399 (2013), and British standard, BSI 12737 (1999), are commonly accepted alternatives for the DCB mode-I fracture test. The compact specimen test methods are particularly attractive for brittle

materials because the crack growth is generally stable, allowing the load-COD curve to be recorded. Test procedures and stress intensity factor with respect to crack length ratio for isotropic materials have been presented in ASTM E 399(2013). The wedge splitting method is a modification of the compact test approach. Proposed by Tschegg and Linsbauer (1986), it is a non-standard fracture test strategy, which introduces a pair of opening forces for a compact specimen by exerting a sharp wedge into a prepared crack to induce mode-I fracture. During testing, the wedge produces both opening forces perpendicular to the crack face, driving crack propagation, and vertical forces parallel to the crack direction, stabilizing crack growth. This method has some outstanding advantages (Stanzl-Tschegg *et al*. 1995). First, it is a very stable test approach and the specimen is compact. Moreover, geometric requirements of the sample are not very stringent. The most attractive characteristic of this method is that it is particularly suitable for testing quasi-brittle materials such as wood and bamboo composites. Considering the advantages of the wedge splitting method, it was used to investigate the mode-I fracture properties of PSB composites in the present work.

EXPERIMENTAL

Materials

PSB composite made from 4-year-old *Phyllostachys sp.*, a common bamboo species cultivated in southeast China, was the test material in this study. Because of the inherently oriented structure of raw bamboo culms (Zhou *et al*. 2012), PSB composite is consequently characterized with orthotropic features and its mechanical properties are very sensitive to fiber orientation (Huang *et al*. 2013). Therefore, in this study, it was treated as transversely isotropic material. A notation scheme adopted by the American standard ASTM E 399 (2013) was introduced to report the orientation of the material and fractures. Following the definition of ASTM E 399, the letters L, T, and S denote the longitudinal (parallel-to-grain), transverse, and short transverse directions of PSB composite, respectively. The orientation of a crack is identified by two letters; the first letter indicates the direction of principal tensile stress, which is always perpendicular to the fracture surface in the mode-I test, while the second denotes the direction of crack propagation. For example, T-L orientation corresponds to loading in perpendicular-to-grain direction and crack propagation in parallel-to-grain direction. Since the fracture of a wedge splitting specimen is usually treated as plane stress problem and the mechanical properties are identical in all directions on the S-T plane, cracks oriented in the T-L and S-L directions may not be identified for mode-I fracture problems; hence the present work only studies T-L oriented fractures. For the purpose of mathematical convenience, the letters L and T were replaced with 1 and 2, respectively, to express the orientations of material and fracture. Mechanical properties of PSB composites involved in this study have been investigated in previous studies and their elastic parameters are presented in Table 1 (Huang *et al*. 2015a).

Table 1. Elastic Parameters of PSB Composite Evolved in this Study

Parameters	Longitudinal Modulus, E_1 (MPa)	Transverse Modulus, E_2 (MPa)	Shear Modulus, μ_{12} (MPa)	Poisson's Ratio, υ_{12}
AVG	11000	3100	1400	0.30
CV	14.4%	18.5%	15.4%	7.2%

Methods

Test principle

The wedge splitting method (BSI 12737 1999) was employed to study mode-I fracture properties of PSB composite in this work. The principle of the test methodology is schematically illustrated in Fig. 1. A test specimen with a rectangular groove and a starter notch at the bottom of the groove are placed on a narrow support fixed on the test machine.

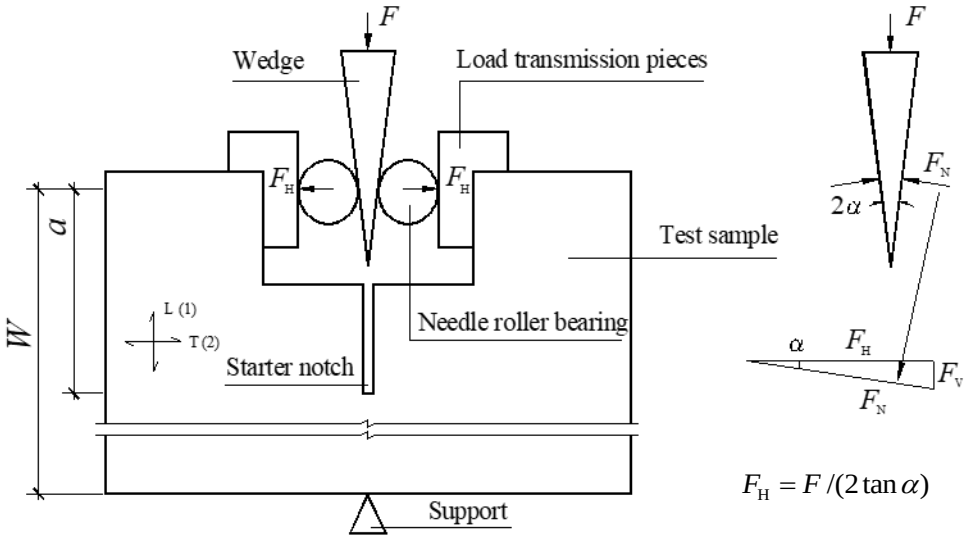

Fig. 1(a). The sketch of wedge splitting test

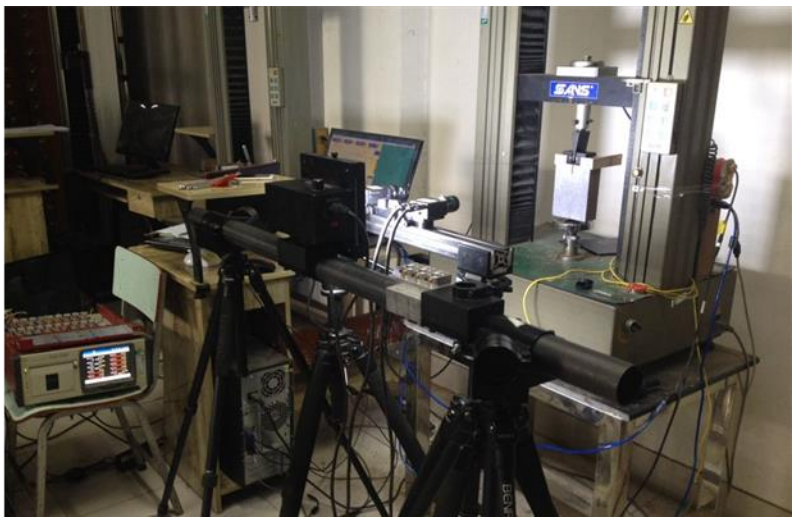

Fig. 1(b). The test setup of wedge splitting test

Needle bearings fixed on load transmission pieces are installed between the wedge and needle bearings. The driving force, *F*, is transmitted from the wedge to the specimen *via* the load transmission pieces. Obviously, *F* can be decomposed into two components, namely the horizontal component, F_H, inducing mode-I fracture and the vertical component, F_V, which helps to stabilize the crack path. The angle of the wedge should be as small as possible so that the influence of the vertical component on the stress of near crack tip may be neglected. Suppose that the wedge angle is 2α and the friction between the wedge and bearings is ignored. Then the crack opening force can be calculated by $F_H = F/(2\tan\alpha)$. Simultaneous recordings of the driving force, *F*, the crack opening displacement (COD), and the load-COD curve, *i.e.*, the F_H-δ curve, can be plotted, where δ=COD.

Determination of KIc

From the viewpoint of theoretical linear elastic fracture mechanics (LEFM), if the plasticity of the near crack tip can be omitted, the energy release rate, *G*, and the values of the J-integral are identical for isotropic materials (Rice 1968). It is well known that the relationship between stress intensity factor, K_I (N.mm$^{-3/2}$), and the value of the J-integral, J_I(N.mm$^{1/2}$), of mode-I fracture for isotropic materials can be expressed as Eq. 1 (Gdoutos 2005),

$$K_I = \sqrt{E' J_I} \tag{1}$$

where $E' = E$ for plane stress (MPa) and $E' = E/(1-\nu^2)$ for plane strain, *E* is Young's modulus (MPa) and ν is Poisson's ratio. Hence the stress intensity factor of isotropic materials for plane problems may be determined by the J-integral. Virtually all test samples were designed with special configurations so that the energy release rate could be easily calculated. The expressions of stress intensity factors associated with the crack depth ratio, $\lambda = a/W$, for standard test samples can be seen in ASTM E 399 (2013), where *a* is the initial crack length (mm) and *W* is the length of total ligament of test specimen (mm), as shown in Fig. 1.

The stress intensity factors for wedge splitting specimens of isotropic material have been numerically investigated by Guinea *et al.* (1996). They offered an expression for calculating K_I using least squares fitting for numerical results. Based on numerous numerical studies, Guinea *et al.* concluded that the stress intensity factors of wedge splitting specimens are very close to those of standard compact specimens provided identical specimen geometry. Thus, the stress intensity factor of the isotropic wedge splitting samples may be calculated by ASTM E 399 (2013) (Eqs. 2 and 3),

$$K_I = \frac{F_H}{B\sqrt{W}} f(\lambda) \tag{2}$$

$$f(\lambda) = \frac{2+\lambda}{(1-\lambda)^{3/2}}\left(0.886 + 4.64\lambda - 13.32\lambda^2 + 14.72\lambda^3 - 5.60\lambda^4\right) \tag{3}$$

where $\lambda = a/W$ is the crack depth ratio.

As an anisotropic composite, the constitutive law of PSB is distinct from isotropic materials. Therefore, Eq. 2 cannot be directly used to compute the stress intensity factor of mode-I fracture in PSB specimens. Kageyama (1989) proposed a method to estimate the stress intensity factor for orthotropic materials, which can be expressed as Eq. 4,

$$K_{\mathrm{I}}^{\mathrm{Orth}} = K_{\mathrm{I}}^{\mathrm{Iso}} f(\lambda, \beta_1, \beta_2) \quad (4)$$

where $K_{\mathrm{I}}^{\mathrm{Orth}}$ and $K_{\mathrm{I}}^{\mathrm{Iso}}$ are mode-I stress intensity factors of orthotropic and isotropic materials, respectively, $f(\lambda, \beta_1, \beta_2)$ is the orthotropic factor which depends on the crack depth ratio, λ , and the material orthotropy, $\beta_1 = E_2 / E_1$ and $\beta_2 = E_1 / \mu_{12}$. However, Kageyama did not provide any method for the orthotropic factor determination.

Sith *et al*. (1965) extended Lehnitskii's (Lekhnitskii 1963) complex expressions for isotropic plane problems to the infinite anisotropy sheet and offered general solutions for crack tip stress fields in anisotropic bodies. By implementing the J-integral calculation for the near tip field of the cracks, they concluded that J_{I} and K_{I} for orthotropic materials have the same form as that of isotropic materials but the material constant in Eq. 1 should be replaced by that in Eq. 5,

$$E' = \sqrt{\frac{2E_1E_2}{\sqrt{E_1 / E_2} - \nu_{12} + E_1 / (2\mu_{12})}} \quad (5)$$

where E_1 and E_2 are Young's moduli along direction-1 and -2, respectively, υ_{12} is Poisson's ratio in the 1-2 plane, and μ_{12} is the shear modulus in the 1-2 plane. Eq. 1 and 5 provide a practical method to determine SIFs for orthotropic composites.

For the wedge splitting samples, SIFs may be determined using Eq.1, provided that the $F_H - \delta$ curve is plotted *via* test, *i.e.*, by determining the critical opening force, F_{Hc} , through experiments, the critical energy release rate can be calculated using Eq. 6,

$$G_{\mathrm{Ic}} = J_{\mathrm{Ic}} = \int_{\Gamma} \left(w_{\mathrm{c}} n_2 - t_{ic} \frac{\partial u_{\mathrm{ic}}}{\partial x_2} \right) d\Gamma \quad (6)$$

where, w_{c} is the strain energy density (MPa) in the domain enclosed by the integral contour Γ , t_{ic} (N) and u_{ic} (mm) are components of traction and displacements on the contour, respectively, and n_i ($i = 1, 2$) are the components of the outward unit vector normal to Γ . In these notations, the subscript, c , represents the items corresponding to the critical opening force, F_{Hc} (N). Furthermore, the parameter K_{Ic} can be calculated using Eq. 1 and 5 by replacing J_I with J_{Ic} .

Determination of crack depth ratio

To obtain valid fracture toughness, the initial crack depth ratio, *a*/*W*, should be chosen carefully so that the effects of remote conditions may be neglected. To this end, near-tip contour integrals for diverse crack depth ratios were implemented using a numerical approach with ABAQUS® software. In the ABAQUS® model (FEM model), the wedge-splitting specimen was treated as a plane stress problem and the material was considered to be orthotropic. The longitudinal direction of the material, *i.e.*, direction-1, was orientated on the y-axis of the model and the transverse direction was along the x-axis, as can be seen in Fig. 2. Material constants were adopted according to Table 1. Cracks were simulated by pre-specified seams, which were supposed to have the same lengths and locations as the starter notches of the test specimens. Because the seam defines an edge of a face with overlapping nodes that can be separated during the analysis process, there is no need to remesh the crack faces as they are separated. To simulate the effect of load transmission, crack opening forces were applied to the real position where the test load

subjected and the distributed coupling technique in ABAQUS ® was adopted. This technique allows for a concentrated load on a reference point to produce an equivalent response of a distributed pressure. An 8-node bi quadratic plane stress element (CPS8R) was chosen to model the specimens. The contour route enclosing the crack tip for the J-integral calculation was specified as shown in Fig.2. Mesh sizes were determined such that the analysis results had little sensitivity to the element density. The vertical component produced by the wedge was omitted due to the small angle of the wedge.

Samples with crack depth ratios ranging from 0.20 to 0.80 were analyzed. The dimensions of the analyzed specimens are illustrated in Fig. 3. In order to evaluate the effect of material anisotropy on SIFs, FEM analyses for both the PSB specimens and their equivalent specimens were implemented to compute J_{I} and K_{I}. An equivalent specimen for an anisotropic specimen is defined by having the same dimensions but having isotropic material properties.

In this study, the longitudinal Young's modulus, E_{I}, and Poisson's ratio, υ_{12}, of the PSB composites were assigned as the Young's modulus, E, and Poisson's ratio, υ, for the equivalent specimens, respectively. The results of the SIFs of both PSB specimens and their equivalent samples are compared in Fig. 4. Discrepancies between the SIFs for isotropic and anisotropic materials can be observed in the case where $\lambda < 0.4$. The SIFs for both the isotropic and anisotropic materials calculated by the FEM model are distinctly different from that calculated by ASTM E 399 when the crack depth ratio is less than 0.4. Once the crack depth ratio exceeds 0.4, the SIFs of both the anisotropic obtained by the

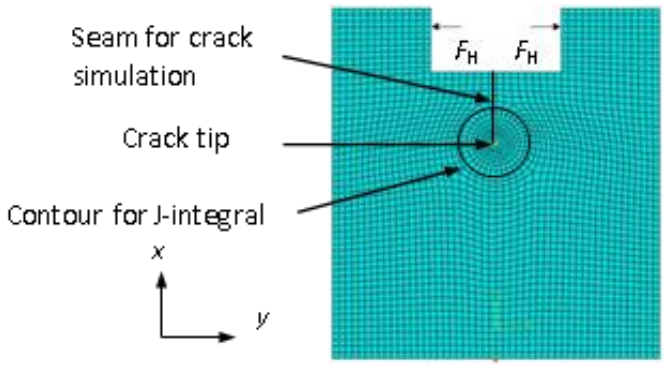

Fig. 2. FEM model for J-integral

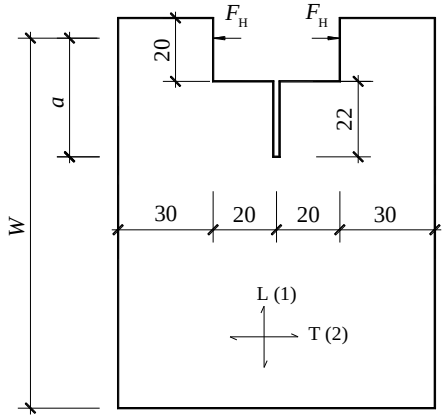

Fig. 3. Configuration and dimensions of specimen

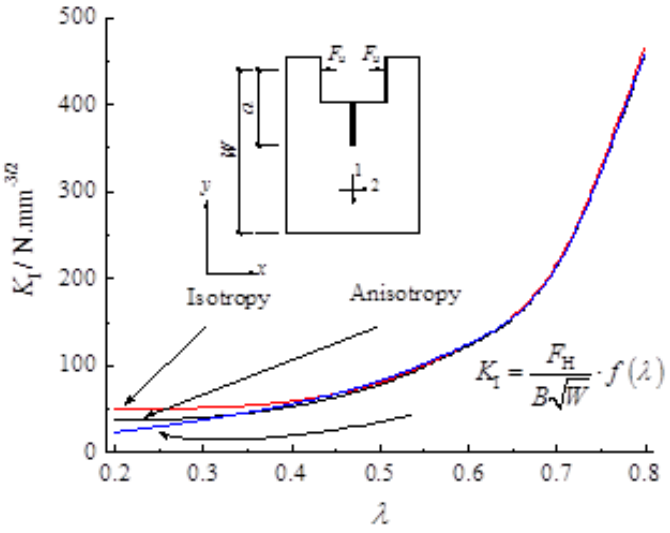

Fig. 4. Comparison of SIFs for PSB specimens and their corresponding equivalent specimens obtained by FEM model and ASTM E 399

FEM model converge to that of ASTM E 399 for isotropic materials. This indicates that the anisotropy of the materials has little effect on the SIFs of mode-I fracture for deep cracks in wedge splitting samples, *i.e.*, $\lambda < 0.4$. Here, K_I may be well estimated by the corresponding formula proposed by ASTM E 399 for compact specimens, as shown in Fig. 4. Furthermore, the results of FEM analysis indicate that the values of the SIFs change less when $\lambda < 0.4$. This implies that the crack depth ratio should never exceed 0.4 and the anisotropy of the material must be considered when the wedge splitting method is used to determine K_{IC}.

Test procedure

According to the results of the numerical studies, the crack depth ratio for wedge splitting specimens should never exceed 0.4, so that the influence of remote conditions may be eliminated. This is somewhat in coincidence with the requirement, $0.45 \le a/W \le 0.55$, for compact test specimens recommended in ASTM E 399. In total, two groups of specimens were tested in this study. The first group, labeled A, was comprised of 15 specimens with different prefabricated crack lengths that were divided into 5 categories according to the crack depth ratio. Specimens were designed according to the instructions of Tschegg *et al*. (1995) and ASTM E 399. The ligament lengths of the test specimens were determined in such a way that the initial crack depth ratio, $\lambda = a/W$ varied from 0.20 to 0.40 increments of 0.05 while the prefabricated crack length, *a*, remained constant. The initial cracks were machined with a band saw with a width less than 2 mm and a starter notch was induced using a razor blade. The configurations and initial crack lengths of the test specimens are illustrated in Fig. 3 and Table 2. The purpose for testing the Group-A samples is to determine the best crack depth ratio for further fracture property testing.

An MTS test machine (Shahai Hao En Hydraul Ic Pressure Technology Co. Ltd, Shanghai, China) of 10 kN capacity and 0.1 N sensitivity was employed to conduct the tests. A digital image displacement acquisition system (VIC-3D) was adopted to record the deformation of the samples during the whole test process. The position and angle of the camera were precisely calibrated to ensure the deformation of the test sample was recorded

accurately. The driving force was monotonically loaded at a speed of 2.0 mm/min until the crack fully expanded. The driving force, *F*, and the deformation for each test sample were simultaneously recorded at a frequency of 5 Hz. The crack opening force can be calculated by $F_{\mathrm{H}} = F/(2\tan\alpha)$. In this study, the wedge angle was 18°; hence $\alpha = 9^{\circ}$. The critical opening force, F_{Hc} (N), from which the prefabricated notch began to expand, was determined using a load-COD curve for each specimen.

By implementing the J-integral *via* Eq. 6 for each specimen that is loaded with a corresponding critical force, F_{Hc}, which is measured by experiments, the SIFs of each sample can be determined (using Eq. 1). The results are presented in Table 2. It can be observed that the critical stress intensity factor, K_{Ic}, measured for categories A-1 to A-4, were almost equal, whereas the results of A-5 deviated greatly from the mean value of the others. Together, considering the experimental results and Tschegg's (1995) suggestion, a crack depth ratio of 0.30 was assigned to the second group (Group-B) of samples, while all other dimensions were the same as Group-A (Fig. 3). The purpose for testing the Group-B samples was to obtain valid fracture toughness and load-COD curves for PSB composites under mode-I fracture. In total, 24 specimens were tested.

Table 2. Dimensions and Test Results of Group-A Specimens

Category	*a*(mm)		*W*(mm)		*a*/*W*		F_{HC} (N)		J_{IC}(N.mm$^{1/2}$)		K_{IC} (N.mm$^{-3/2}$)	
	Mean	CV.	Mean	CV.	Mean	CV.	Mean	CV.	Mean	CV.	Mean	CV.
A-1	35.92	0.38%	179.25	0.03%	0.20	0.36%	3550.68	5.53%	0.437	14.03%	39.11	7.18%
A-2	36.55	1.19%	145.20	0.11%	0.25	1.08%	3123.90	15.05%	0.553	9.04%	39.48	14.73%
A-3	36.42	1.87%	121.69	0.28%	0.30	2.14%	2659.80	6.05%	0.351	11.43%	35.10	5.82%
A-4	36.40	1.89%	104.96	0.42%	0.35	1.46%	2467.27	7.74%	0.384	15.28%	36.66	7.82%
A-5	36.63	0.04%	92.04	0.35%	0.40	0.31%	1529.14	7.96%	0.200	16.55%	26.41	8.09%

The test procedure used for Group-B was as same as that for Group-A. The results of the specimens whose load-COD curves were not fully recorded or the cracks apparently deviated from their original orientation were abandoned. The results of 12 specimens were accepted. The critical stress intensity factor was very close to that for Group-A specimens with a crack depth ratio of 0.3. Table 3 compares the fracture toughness of the PSB composites with that of commonly used building construction wood (Smith *et al*. 2003). It can be concluded that the fracture toughness of PSB composites is higher than that of wood materials commonly used in construction.

Table 3. Fracture Toughness for PSB Composite and the Commonly Used Wood

Materials	E_1 (MPa)	E_2 (MPa)	μ_{12} (MPa)	K_{IC} (N.mm$^{-3/2}$)
PSB	11000	3100	1400	34.98
Douglas-fir	12300	615	960	26.78
Western white pine	10100	384	485	7.91
Northern red oak	12500	1025	1013	12.97
Yellow-poplar	10900	469	752	16.35

E_1, longitudinal modulus, E_2, transverse modulus, μ_{12}, shear modulus, K_{IC}, stress intensity factor

RESULTS AND DISCUSSION

Fracture Mechanism

Experimental load-COD curves plotted in Fig. 5 show that the load-COD response exhibited a nonlinear region prior to the peak load followed by a strain-softening region after the peak. This phenomenon is similar to wood and has been confirmed by Simth *et al.* (2003) as a quasi-brittle behavior induced by the nonlinear response of the fracture process zone (FPZ) near the crack tip. As previously mentioned, PSB composite has distributed inherent microvoids and fine cracks. Once an undamaged PSB specimen is loaded, microvoids start to grow and coalesce, leading to small cracks. As these small cracks accumulate, the compliance of the test sample increases and the load-COD curve deviates from linear behavior. Prior to peak load there is a localization process in which the damage causing failure becomes confined to a narrow region. By the time the peak is reached, a critical crack accompanied by the FPZ has been established and strain softening can occur. The existence of FPZ causes energy to be dissipated more gradually than for brittle failure. The toughening mechanism interpreted above can be demonstrated by Fig. 7, which depicts a typical failure mode of a specimen. It can be observed that there were some sub-cracks left around the path of the main crack.

Another toughening mechanism is debonding and fiber bridging. Indeed, PSB is composed of a large amount of bamboo fibers glued together with resin. Crack extension always happens in the direction of fiber orientation and virtually all damage occurs between the interface of fiber and resin. Similar to other fibrous composites, damage that occurs in the fibers' interfaces invariably causes debonding and fiber bridging in crack extension. A SEM image presented in Fig. 7(a) shows a debonded surface of a specimen. Matrix breakage can be observed at the surface. The breakage of fiber bridges and micro fractures can be seen in Fig. 7(b). Furthermore, the crack may deviate from its original orientation in the case where it encounters a micro-crack or where the fibers are in the unparallel-to-grain (cross) direction. Therefore, in most cases the crack is not fully self-similar crack.

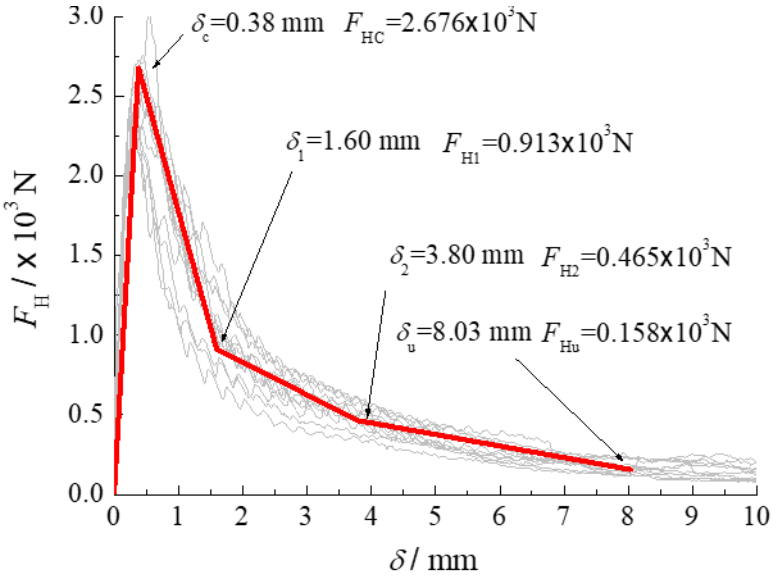

Fig. 5. Load-COD curves. The gray lines are obtained by tests; the red one is modeling line

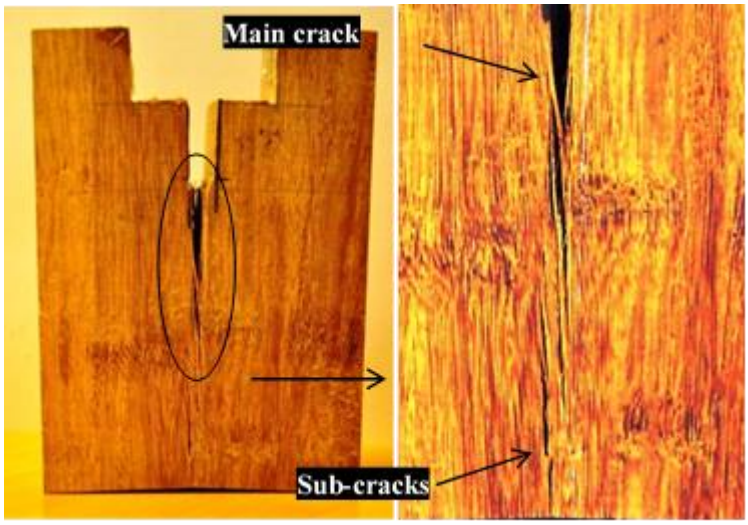

Fig. 6. Sub-cracks in the vicinity of main crack tip

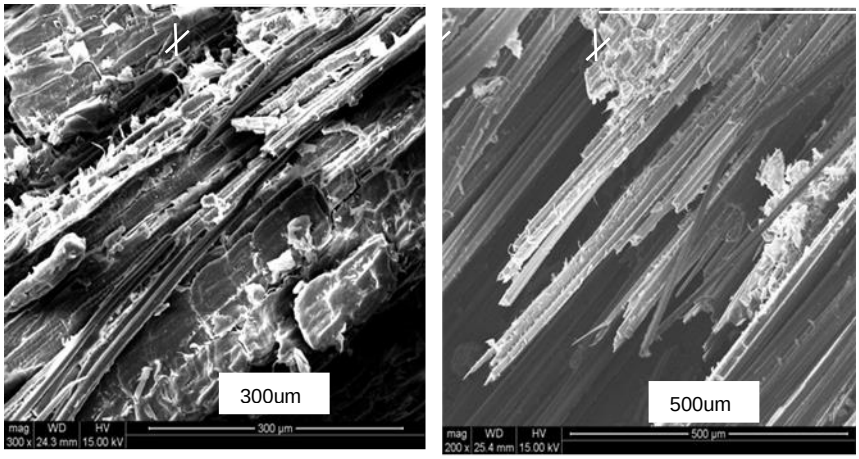

Fig. 7. Micro images of broken surface. (a) Debonding; (b) fiber breakage

Load-COD Curves

Unless otherwise stated, the discussions hereinafter are all based on the experimental results of Group-B. Figure 5 presents the curves of crack opening force *vs.* its associated displacements, *i.e.*, the load-COD curve of each specimen. The peak point of each curve was determined by the data reduction method prescribed in ASTM E 399. For the sake of convenience, a multi-line to model load-COD curve based on the average of experimental results was adopted to evaluate the energy release rate. Figure 5 illustrates a tri-linear model for the strain softening behavior for post-peak curves. The crack opening force, F_H, and its corresponding COD, δ, for each inflection point of the tri-linear model are also illustrated in Fig. 5. Because at the end of crack extension the crack tip is close to the support the test sample, the near-tip field is significantly affected by boundary conditions. Thus, the data from the end of the crack extension should be abandoned since it is unreliable in the evaluation of fracture properties. The crack lengths corresponding to each turning point of the tri-linear model are presented in Fig. 8.

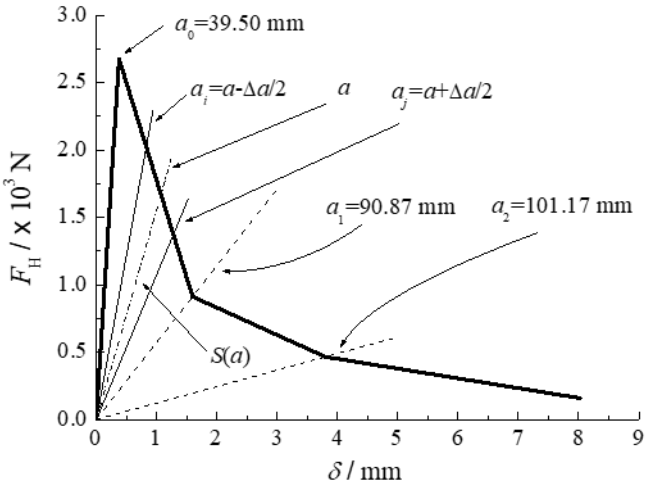

Fig. 8. Sketch of the elastic energy release rate evaluation. $G_R(a) = S(a) / B\Delta a$

R-Curve

The energy resistance curve, known as the *R*-curve, is characterized as an energy consumption per unit area when a crack extending to an infinitesimal length (Anderson 2005). According to Griffith's (1920) theory, strain energy available for crack extension in perfectly elastic media is exactly consumed to create a new surface, that is, the resistance force is exactly equal to the crack driving force; hence for ideally brittle fracture, $G_R = G$, where G and G_R are energy release rate and crack resistance energy, respectively. The general relationship between energy release rate and crack resistance energy may be expressed as Eq. 7 according to the energy balance principle (Griffith 1920),

$$G_R = G + \frac{dU}{da} \tag{7}$$

where U is the total energy of the media with a crack (MPa).

Because microvoids, fine cracks, and fiber-bridges exist in the crack front, to exactly measure the crack length is not easy in practice. In fact, the physical mechanism of fracture, such as crack bridging, emphasizes that LEFM cannot be directly applied to quasi-brittle failures (Morel *et al*. 2005). Although Irwin's modification includes a plastic energy term, there are still limitations for the energy balance approach in determining the conditions required for instability of an ideally sharp crack. The energy balance approach presents insuperable problems for many practical situations, especially for slow stable crack extension (Griffith 1920). Nevertheless, an adaptation of LEFM, referred to as an equivalent linear elastic approach (Morel *et al*. 2005), can provide a useful approximation of the quasi-brittle behavior. On the basis of equivalent LEFM, the equivalent crack length is understood to be the crack length of the specimen which gives the same compliance as the real one. In other words, the crack lengths have a one-to-one relationship with compliance of crack cantilever. Hence the real crack length may be evaluated using the equivalent crack length in accordance with its associated compliance.

According to equivalent LFEM theory, an R-curve may be directly evaluated from the load-COD curve (Morel *et al*. 2005). Referring to Fig. 8, a radial line (compliance line) going through the origin of the coordinate plane in the load-COD diagram represents a load-displacement response for a specific crack length; hence, the reciprocal tangent of the

line gives the compliance associated with the crack length. Suppose that a crack of length a_i extends Δa to length a_j, the area enclosed by the corresponding compliance lines associated with a_i and a_j and the load-COD curve equals the energy available for crack growth. Provided that Δa is small enough, the crack resistance force may be evaluated using Eq. 8 (Gdoutos 2005),

$$G_R(a) = \frac{1}{2B\Delta a}(F_i\delta_j - F_j\delta_i) \quad (8)$$

where F and δ are the crack opening force and displacement, respectively. Because the energy evaluation of this approach is based on the load-COD curve, the energy dissipation due to inelastic responses and microvoids coalescing are included, hence it is particularly suitable for quasi-brittle materials.

To construct an R-curve for PSB composites under mode I fracture, the compliance, C, associated with a crack of length a was numerically evaluated by FEM analysis for all tests specimens. Figure 9 illustrates the results of the FEM analyses and corresponding empirical equation for $C(a)$. For a given point on the load-COD curve, the compliance may be calculated using the experimental load and displacement, and the corresponding equivalent linear elastic crack length may be computed using a stationary interactive method using the empirical compliance equation C(a). In the present study, the crack extension increment Δa was set to be about 1% of the initial crack length according to the suggestion of Morel (2005). Because ignoring residual deformations in the FPZ leads to a deviation in the calculation of compliance from the actual value, the compliance for each calculation step should be corrected in line with the initial compliance, $C(a_0)$.

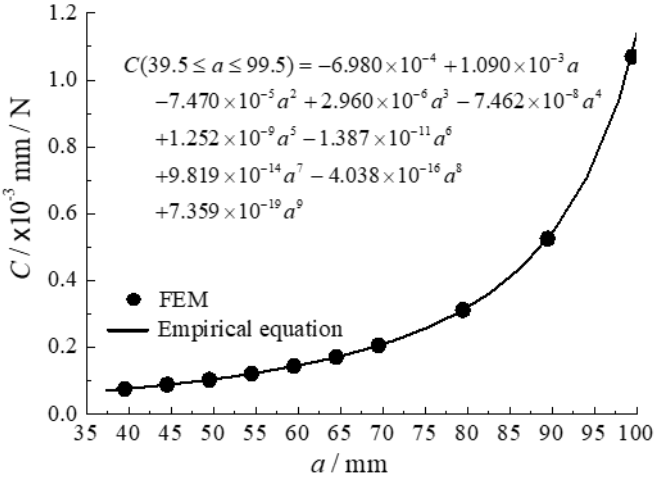

Fig. 9. Compliance of crack cantilever vs. crack length

The R-curve (crack resistance force *vs.* the equivalent crack length) obtained using the aforementioned method can be seen in Fig. 10. The R-curve first exhibits rising behavior until the critical crack length (a_c=87.95 mm) is reached. However, the post peak R-curve obtained in this study differs from what is expected for an R-curve of quasi-brittle material like wood.

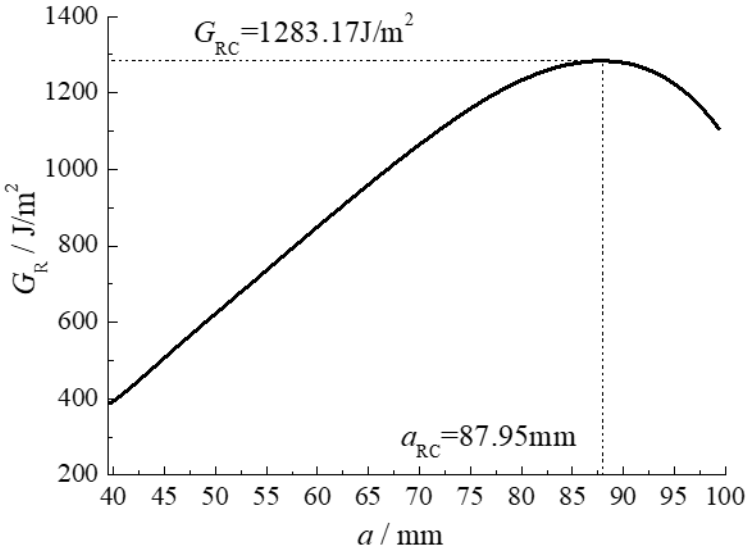

Fig. 10. R-curve

The expectation is that the resistance of crack growth becomes independent of equivalent crack length after the critical crack length is reached (Morel *et al*. 2012). The interpretation of the rising behavior of the R-curve is that crack toughening is relative to the growth of the FPZ attached to the notch tip leading to an increase in crack resistance with the augment of equivalent crack length. When the FPZ reaches its critical length, the main crack propagates with its critical FPZ and this propagation corresponds to a constant crack resistance. Hence, a levelling off R-curve for post critical crack expansion may be observed.

It can be concluded from the above that the rising R-curve indicates that the toughening mechanisms of PSB composites are similar to those of wood materials. The equivalent length of FPZ may be obtained by $l_{FPZ} = a_c - a_0$. Figure 10 shows that the FPZ is the major toughening mechanism of fracture for PSB composites.

The R-curve is geometry-dependent, and only the crack tip dominated by the plane strain state can provide stable crack resistance (Dorado *et al*. 2008). Hence an R-curve cannot be considered as an intrinsic fracture characteristic of a material (Lartigau *et al*. 2015). Indeed, the small crack always becomes located in the cantilever or in the main crack-front after the main crack growth; thus the compliance evaluated by linear FEM model may significantly derivate from the real value. On other hand, crack extension in PSB composites strongly depends on the fiber orientation and microstructures of the material. The crack may deviate from its initial direction once it encounters a micro-crack or fibers not parallel to its original orientation. Because of this, it is quite difficult to recognize a crack tip without vagueness. The above discussions are probably the reasons why the post R-curve exhibits descending behavior in this study.

CONCLUSIONS

1. Parallel stand bamboo (PSB) is a new type of wood-like bamboo composite. Experimental investigation in this study suggests the mode-I fracture toughness of PSB

composite is much higher than that of commonly used wood materials in construction engineering.

2. Load-COD diagrams of wedge splitting test specimens exhibit a pronounced nonlinear region prior to the peak load followed by a strain-softening region after the peak. This phenomenon reveals that the fracture of PSB composite presents quasi-brittle behavior. Microvoids coalescence and small crack accumulation are the major mechanisms of the near-tip FPZ, which leads to increasing compliance of the test sample and deviation of the load-displacement response from linear behavior prior to the peak load.
3. Crack extension of a PSB composite is hardly perfectly self-similar, depending on the fiber orientation and microstructures of the material relative to the path by which the crack propagates through. The crack may deviate from its original orientation once it encounters a micro-crack or fibers unparallel to its original orientation. Furthermore, virtually all growths of the main cracks are accompanied by the extension of sub-cracks in the vicinity of the crack tip; hence it is quite difficult to recognize the crack tip without vagueness.
4. The R-curve of PSB composites obtained in this study first exhibited rising behavior until the critical crack length was reached. The post peak R-curve exhibited descending behavior contrary to that of common quasi-brittle materials, which present a plateau in post-peak crack extension.

ACKNOWLEDGMENTS

This research was supported by the National Science Fund of China (No. 51578291), National Key Research Project (No. 2017YFF0207203-04), National Demonstration Project of Forestry Science and Technology, and the Priority Academic Development Program of Jiangsu Higher Education Institutions.

REFERENCES CITED

Anderson, T. L. (2005). *Fracture Mechanics: Fundamentals and Applications*, CRC Press, Boca Raton, FL, USA.

ASTM E 399 (2013). "Standard test method for linear-elastic plane strain fracture toughness KIC of metallic materials," ASTM International, West Conshohocken, PA.

BS EN ISO 12737 (1999). "Metallic materials: Determination of plane-strain fracture toughness," British Standards Institution, London, UK.

Dorado, N., Morel, S., M. F. S. F, Moura de, Valentin G., and Morais, J. (2008). "Comparison of fracture properties of wood species through cohesive crack simulations," *Composites: Part A* 39 (2008), 415-427. DOI: 10.1016/j.compositesa.2007.08.025

Gdoutos, E. E. (2005). *Fracture Mechanics: An Introduction*, Springer, Berlin, Germany.

Griffith, A. A. (1920). "The phenomena of rupture and flow in solids," *Philosophical Transactions* 221, 163-198.

Guinea, G. V., Elces, M., and Planas, J. (1996). "Stress intensity factors for wedge-splitting geometry," *International Journal of Fracture* 81(2), 113-124.

Hearmon, R. F. S. (1969). *An Introduction to Applied Anisotropic Elasticity*, Oxford University Press, Oxford, UK.

Huang, D., Zhou, A., and Bian, Y. (2013). "Experimental and analytical study on the nonlinear bending of parallel strand bamboo beams," *Construction and Building Materials* 35(3), 585-592. DOI: 10.1016/j.conbuildmat.2013.03.050

Huang, D., Bian, Y., Zhou, A., and Sheng, B. (2015a). "Experimental study on stress-strain relationships and failure mechanisms of parallel strand bamboo made from *Phyllostachys*," *Construction and Building Materials* 77(2015), 130-138. DOI: 10.1016/j.conbuildmat.2014.12.012

Huang, D., Bian, Y., Huang, D. M., Zhou, A., and Sheng, B. (2015b). "An ultimate-state-based-model for inelastic analysis of intermediate slenderness PSB columns under eccentrically compressive load," *Construction and Building Materials* 94(2015), 306-314. DOI: 10.1016/j.conbuildmat.2015.06.059

Iwrin, G. R. (1956). "Onset of fast crack propagation in high strength steel and aluminum alloys," in: *Proceedings of the Sagamore Research Conference*, New York, USA, pp. 289-305.

Kageyama, K. (1989). "Fracture mechanics of notched carbon/epoxy laminates," in: *Application of Fracture Mechanics to Composite Materials*, K. Friedrich (ed.), Elsevier, Amsterdam, Netherlands, pp. 327-396.

Lartigau, J., Coureau, J. L., Morel, S., Galimard, P., and Maurin, E. (2015). "Mixed model fracture of glued-in rods in timber structures: A new approach based on equivalent LEFM," *International Journal of Fracture* 192 (1), 71-86. DOI: 10.1007/s10704-014-9986-9

Lekhnitskii, S.G. (1963). *Theory of Elasticity of an Anisotropic Body*, Holden-Day. MIR. Publishers, Moscow, Russia.

Morel, S., Bouchaud, E., Schmittbuhl, J., and Valentin G. (2012). "R-curve behavior and roughness development of fractures surfaces," *International Journal of Fracture* 114(4), 307-325.

Morel, S., Dourado, N., Valentin, G., and Moriais, J. (2005). "Wood: A quasibrittle material R-curve behavior and peak load evaluation," *International Journal of Fracture* 131(4), 385-400. DOI: 10.1007/s10704-004-7513-0

Rice, J. R. (1968). "A path independent integral and the approximate analysis of strain concentration by notches and cracks," *Journal of Applied Mechanics* 35(2), 379-386.

Smith, I., Landis, E., and Gong, M. (2003). *Fracture and Fatigue in Wood*, John Wiley and Sons, Hoboken, NJ, USA.

Sith, G. C., Paris, P. C., and Irwin, G. R. (1965). "On cracks in rectilinearly anisotropic bodies," *International Journal of Fracture Mechanics* 1(2), 189-203.

Stanzl-Tschegg, S. E., Tan, D. M., and Tschegg, E. K. (1995). "New splitting method for wood fracture characterization," *Wood Science and Technology* 29(1), 31-50. DOI: 10.1007/BF00196930

Tschegg, E. K., and Linsbauer, H. N. (1986). "Test method for the determination of fracture mechanics properties," Austrian Patent No. A-233/86390238.

Williams, M. L. (1952). "Stress singularities resulting from various boundary conditions angular corners of plated in extension," *Journal of Applied Mechanics* 19(1), 526-528.

Williams, M. L. (1956). "On the stress distribution at the base of a stationary crack," *Journal of Applied Mechanics* 24(1956), 109-114.

Williams, J. G. (1989). "Fractures of anisotropic materials," in: *Application of Fracture Mechanics to Composite Materials*, K. Friedrich (ed.), Elsevier, New York, NY, USA, pp. 3-38.

Zhou, A., Huang, D., Li, H., and Su, Y. (2012). "Hybrid approach to determine the mechanical parameters of fibers and matrixes of bamboo," *Construction and Building Materials* 35(10), 191-196. DOI: 10.1016/j.conbuildmat.2012.03.011

Article submitted: October 17, 2017; Peer review completed: February 16, 2018; Revised version received: March 23, 2018; Accepted: March 24, 2018: Published: April 17, 2018.
DOI: 10.15376/biores.13.2.3905-3921